Numerical Evidence for Thermally Induced Monopoles

P. Wirnsberger,[1] D. Fijan,[1,2] R. A. Lightwood,[1] A. Šarić,[1,3] C. Dellago,[4] and D. Frenkel[1, a)]

[1)]*Department of Chemistry, University of Cambridge, Cambridge CB2 1EW, United Kingdom.*

[2)]*Current address: Department of Chemistry, University of Oxford, Oxford OX1 3QZ, United Kingdom.*

[3)]*Current address: Department of Physics and Astronomy, Institute for the Physics of Living Systems, University College London, WC1E 6BT, United Kingdom.*

[4)]*Faculty of Physics, University of Vienna, 1090 Vienna, Austria.*

Electrical charges are conserved. The same would be expected to hold for magnetic charges, yet magnetic monopoles have never been observed. It is therefore surprising that the laws of non-equilibrium thermodynamics, combined with Maxwell's equations, suggest that colloidal particles heated or cooled in certain polar or paramagnetic solvents may behave as if they carry an electrical/magnetic charge[1]. Here we present numerical simulations that show that the field distribution around a pair of such heated/cooled colloidal particles agrees quantitatively with the theoretical predictions for a pair of oppositely charged electrical or magnetic monopoles. However, in other respects, the non-equilibrium colloids do not behave as monopoles: they cannot be moved by a homogeneous applied field. The numerical evidence for the monopole-like fields around heated/cooled colloids is crucial because the experimental and numerical determination of forces between such colloids would be complicated by the presence of other effects, such as thermophoresis.

The existence of quasi-monopoles in a system of heated or cooled colloids in a polar or paramagnetic fluid follows directly from non-equilibrium thermodynamics, combined with the equations of electro/magneto-statics[1]. Although suggested theoretically, they have thus far not been studied experimentally. The present paper provides numerical evidence indicating that the predicted effects are real and robust. In what follows, we consider the case of thermally induced quasi-monopoles in a dipolar liquid, but all our results also apply to paramagnetic liquids. It has been shown that a thermal gradient will create an electrical field in a liquid of dipolar molecules with sufficiently low symmetry[2,3]. In the absence of any external electric field, a heated or cooled colloid placed in such a liquid, will generate the field[2,4,5]

$$\boldsymbol{E}_{\mathrm{TP}}(\boldsymbol{r}) = S_{\mathrm{TP}} \nabla T(\boldsymbol{r}), \qquad (1)$$

where $T(\boldsymbol{r})$ is the temperature and S_{TP} the thermo-polarisation coefficient, with a magnitude that is not known *a priori*. For water near room temperature, S_{TP} has been estimated to be $S_{\mathrm{TP}} \approx 0.1$ mV/K[4,6].

Let us next consider the electrical polarisation around a heated (or cooled) colloidal particle. In steady state the temperature profile at a distance r from the centre of an isolated, spherical colloid of radius R satisfies

$$T(r) = T_\infty + (T_R - T_\infty)\frac{R}{r}, \qquad (2)$$

and hence

$$\boldsymbol{E}_{\mathrm{TP}}(\boldsymbol{r}) = -S_{\mathrm{TP}}(T_R - T_\infty)\frac{R}{r^2}\hat{\boldsymbol{r}}, \qquad (3)$$

where T_∞ is the temperature in the bulk liquid and $\hat{r}$ the radially outward pointing unit vector. Note that E_{TP} decays as $1/r^2$. Using Gauss's theorem, we can then write

$$\oiint \boldsymbol{E}_{\mathrm{TP}}(\boldsymbol{r}) \cdot \mathrm{d}\boldsymbol{S} = -4\pi S_{\mathrm{TP}}(T_R - T_\infty)R \equiv \frac{q_{\mathrm{TP}}}{\epsilon_0}, \qquad (4)$$

where ϵ_0 is the dielectric permittivity of vacuum. In words: the flux through a closed surface around a neutral colloid is non-zero, and is equal to the flux due to an apparent charge $q_{\mathrm{TP}} = -4\pi\epsilon_0 S_{\mathrm{TP}}(T_R - T_\infty)R$. Note that the effective charge is proportional to the radius of the particle, hence larger colloids will have a larger apparent charge.
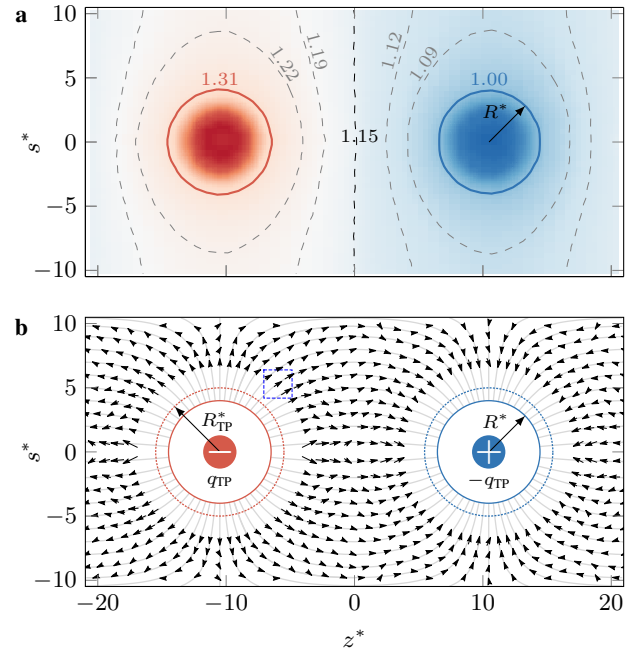

FIG. 1. **a** Cylindrically averaged temperature profile with symmetry axis z^*, perpendicular direction s^*, and isosurfaces (solid and dashed lines) around two colloids of radius R^*, one heated and the other one cooled. **b** Cylindrically averaged field lines generated by two point charges, $\pm q_{\mathrm{TP}}$, with periodic boundary conditions. The superimposed arrows indicate the average dipolar orientations obtained from the simulations. Averages were calculated inside small volumes (dashed rectangle). To avoid spurious boundary effects, we did not consider dipoles within a radius R^*_{TP} from the center of either colloid.

a)Corresponding author: df246@cam.ac.uk

To verify the existence of thermally induced charges numerically, we performed non-equilibrium molecular dynamics (NEMD) and equilibrium MD simulations of a heated and a cooled colloid immersed into a modified ('off-centre') Stockmayer fluid[7], consisting of particles with a point dipole and a Lennard-Jones (LJ) centre displaced along the direction of the dipole moment (Appendix A). This displacement is controlled by a parameter α. A non-zero value of α is necessary to observe the effect[3], as molecules would otherwise have no preferred thermo-molecular orientation. An important property of our model fluid is that S_{TP} is effectively constant in the temperature and density range investigated (Appendix C), thereby facilitating the analysis as compared to the polar models considered previously[2,4,6,8–12]. The temperature gradient is sustained by continuously pumping energy into the hot colloid and removing it from the cold one such that the overall system energy is constant[13].

In our numerical simulations, we chose a geometry in which the two colloids are located on the z-axis in a system with periodic boundary conditions. As a first test of the theory, we measured two-dimensional steady state profiles for the temperature and the average dipolar orientations, both shown in Fig. 1. Quantities labeled with an asterisk are expressed in reduced units, defined in the *Methods* section. To improve statistics, we computed cylindrical averages (indexed by z and s), although the underlying problem does not exhibit full radial symmetry in the xy–plane due to effects of periodic boundary conditions. However, as the theoretical predictions were also cylindrically averaged, the comparison between simulation and theory is still valid. The dashed vertical line going through the origin of Fig. 1a corresponds to the equilibrium (or bulk) temperature T_∞. With the temperature values of the specific contour lines shown in the figure and a value of $S_{\mathrm{TP}}^* = (0.216 \pm 0.022)$ computed in the vicinity of the origin (Appendix C), we can employ equation (4) to obtain an estimate of $q_{\mathrm{TP}}^* \approx -0.14$ for the thermally induced charge. If we use the LJ parameters of SPC/E water[14] for the unit conversion, this corresponds to $q_{\mathrm{TP}} \approx 5.4 \times 10^{-3} q_e$, where q_e is the charge of an electron.

Figure 1b shows the average dipolar orientations superimposed onto the field lines generated by two virtual point charges located at the centres of the colloids. To single out the thermally induced alignment from contributions already present in equilibrium, e.g. the alignment caused by surface layering of solvent molecules in the vicinity of the colloids, we measured equilibrium orientations in a separate simulation and subtracted them from the non-equilibrium result. This procedure assumes that the coupling between the various contributions to the total field is negligible. We found this assumption to be reasonable everywhere apart from the immediate vicinity of the colloids. Therefore we excluded the first layer of solvent molecules, i.e. all particles within a distance of $R_{\mathrm{TP}}^* = 5$ from the colloid centres, from the averaging. The precise value of R_{TP} does not matter as long as it is chosen sufficiently large. We picked the smallest value that allows us to single out the effect. As we can see, the dipoles are aligned very well with the field lines generated by two point charges in a periodic system.

As a more quantitative test of the theory, we measured the electric field induced by the temperature gradient. To improve the statistical accuracy of our results, we average the field over planes perpendicular to the symmetry axis, such that all contributions apart from $E_{z,\mathrm{TP}}$ cancel out. The system behaves as if the two charges of opposite sign are distributed over thin spherical shells of radius R_{TP}, as depicted in Figs 2a and b. For this geometry, we obtain the analytical solution for the electrical field (see Appendix A):

$$\frac{\langle E_{z,\mathrm{TP}}(z) \rangle}{\tilde{E}} = \begin{cases} -1 & \text{if } |z| > z_{\mathrm{c}} + R_{\mathrm{TP}}, \\ +1 & \text{if } |z| < z_{\mathrm{c}} - R_{\mathrm{TP}}, \\ (z - z_{\mathrm{h}})/R_{\mathrm{TP}} & \text{if } |z - z_{\mathrm{h}}| \leq R_{\mathrm{TP}}, \\ (z_{\mathrm{c}} - z)/R_{\mathrm{TP}} & \text{otherwise,} \end{cases} \quad (5)$$

where $z_{\mathrm{h/c}} = \mp L/4$ denote the locations of the hot and cold colloid, respectively, L is the box length in the z-direction, $\tilde{E} = q_{\mathrm{TP}}/(2A\epsilon_0)$ is the constant value of the averaged field between the colloids, and $A = L^2/4$ is the cross-sectional area. The left-hand side of the above expression can be related to the average dipole density such that[6]

$$\langle E_{z,\mathrm{TP}}(z) \rangle = -\frac{\langle \rho_\mu(z) - \bar{\rho}_\mu \rangle}{\epsilon_0}, \quad (6)$$

where $\bar{\rho}_\mu = 1/L \int \mathrm{d}z \langle \rho_\mu(z) \rangle$ is the box average of $\langle \rho_\mu(z) \rangle$. Equation (6) enables us to link the theory and NEMD simulations quantitatively. We can estimate the right-hand side of the above equation readily by sampling the instantaneous dipole orientations and performing temporal and spatial averaging for slabs perpendicular to the symmetry axis. Using equation (5), we can then infer the value of $\tilde{E}$ from our results and obtain an independent numerical estimate of q_{TP}, in addition to the one provided by equation (4). Observing a good agreement for both estimates would provide strong support for the theory, since it would suggest that Gauss's theorem can be applied to arbitrary volumes enclosing the colloids, just as if they carried real Coulomb charges. We note, however, that there is an important conceptual difference between estimating the charge using equation (5) versus equation (4): the latter already *assumes* that equation (1) holds whereas the former *validates* it.

Figure 2c shows the steady state result for the spatial variation of the averaged field calculated according to equation (6). Equilibrium averages were subtracted and solvent particles within a distance of R_{TP} from the colloid centres excluded from the averaging, which makes the effective radius of the charge distribution essentially an input parameter of our model. We can see that the simulation data are in excellent agreement with the theoretical expression (5): the average field is constant in the fluid region and changes linearly within a distance of R_{TP} from the colloid centre. From the plateau in the centre we estimate $\tilde{E}^* = (-1.96 \pm 0.20) \times 10^{-3}$ for the regions where the field is constant, and find a value of $q_{\mathrm{TP}} = (5.27 \pm 0.54) \times 10^{-3} q_e$ for the thermally induced charge. Both estimates for q_{TP} are in excellent agreement. The sign of q_{TP} can be controlled either by changing the rate of energy, $\mathcal{F}$, supplied to or withdrawn from the colloid (flipping hot and cold) or by changing α, such that $\mathrm{sgn}(q_{\mathrm{TP}}) = \mathrm{sgn}(\alpha)\,\mathrm{sgn}(\mathcal{F})$.

A key question is whether the effective electrical or magnetic charge of colloidal monopoles can be measured in experiments. The present simulations suggest that, at the very least the effect of the monopole fields on probe charges (or dipoles) should be observable. Of course, it would be attractive to make the effect
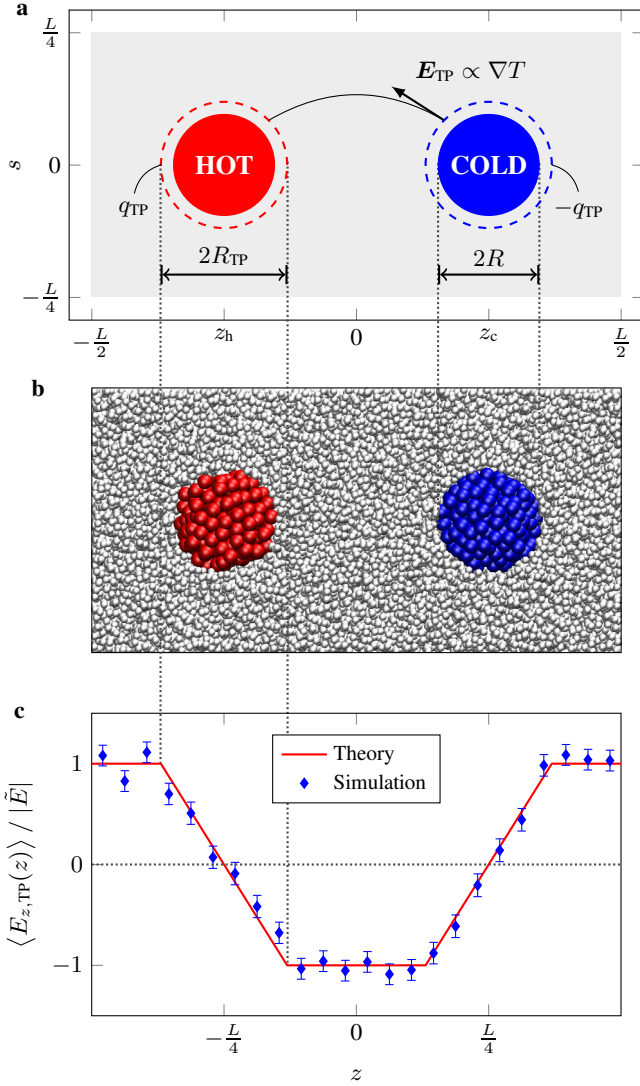
FIG. 2. **a** Illustration of the setup. The dashed lines of radius R_{TP} enclosing the hot and cold colloids represent infinitesimally thin spherical shells carrying the induced charges $\pm q_{TP}$. The black solid line illustrates a field line and the arrow represents a field vector. **b** A typical configuration obtained from simulation showing the colloids immersed into the solvent particles. **c** Thermally induced field averaged over slabs perpendicular to the symmetry axis. The simulation results (blue symbols) were calculated from the averaged dipole density excluding two balls of radius R_{TP} centred around the colloids. The solid line shows the theoretical prediction given by equation (5). The dotted vertical and horizontal lines were added to guide the eye and to highlight the symmetry of the induced field.

as large as possible by increasing the temperature difference between the particle and the solvent. However, the temperature range is limited by the fact that extreme heating or cooling will bring the system out of the linear-response regime - and possibly even induce phase transitions in the solvent. Moreover, the colloidal monopoles differ in an important respect from true monopoles: they cannot be moved by a uniform external field[1]. It is therefore tempting (be it slightly frivolous) to call such colloidal monopoles 'quacks', as they quack like a duck (i.e. they create a field similar to that of a real monopole), but they don't

swim like a duck (they cannot be used to transport charge). One of the main effects that may obscure observation of the Coulomb-like interaction between oppositely heated colloids is thermophoresis, which will also cause colloids to move in the temperature gradient caused by another colloid. However, at least in the linear regime, this effect should cause otherwise identical but oppositely heated colloids to move *in the same direction* with respect to the fluid rather than with respect to one another. Finally, there are many open questions about the practical consequences of the existence of thermal monopoles. It is, for instance, conceivable that such particles in an electrolyte solution will get 'decorated' with real charges, and thereby acquire real charge (opposite and equal to the 'thermal' charge) that can be dragged along. That charge should respond to a uniform external field: the resulting electro-osmotic flow would cause motion of the colloids.

ACKNOWLEDGEMENTS

AUTHOR CONTRIBUTIONS

The research was planned by P. W., C. D. and D. F. based on a theoretical suggestion by D. F. Simulations were carried out by P. W. with assistance of R. A. L., D. Fijan and A. Š. The manuscript was written by P. W., A. Š., C. D. and D. F.

METHODS

Simulation setup. All equilibrium and non-equilibrium MD simulations were performed using the software package LAMMPS[15] (version 14Jun16). We employed a fully periodic rectangular simulation box with dimensions $(L_x, L_y, L_z) = (L/2, L/2, L)$, where $L = 41.93\sigma$, containing 13422 solvent particles of LJ diameter σ, which defines the unit of length, and two colloids centred at $r_{h/c} = (0, 0, \mp L/4)$. Each colloid was modelled with an elastic network of 201 beads with 2808 harmonic springs connecting nearest, second-nearest and third-nearest neighbours. The initial colloid configuration was cut out of an fcc lattice with a density of $0.75/\sigma^3$ matching the solvent density. Springs were then added to all beads within a distance of $R = 4\sigma$ of the centre of mass positions of the two colloids. The equilibrium distances of the harmonic spring potentials were taken to be the initial bead separations and the spring constant was set to $5\epsilon/\sigma^2$, where the LJ parameter ϵ defines the energy scale. During the simulation the colloids were held in place by two additional stiff harmonic springs ($100\epsilon/\sigma^2$) tethering the centres of mass to the equilibrium positions. The solvent molecules were modelled as modified Stockmayer particles consisting of a point dipole, located at the particle's centre of mass, and a shifted LJ centre. We displaced the LJ centre from the dipole by $\Delta r = \alpha\hat{\mu}$, where $\alpha = -\sigma/4$ controls

the asymmetry and $\hat{\boldsymbol{\mu}}$ is the unit vector of the dipole moment $\boldsymbol{\mu}$. This modification leads to additional torque contributions which are summarised in Appendix B. We used the relations $\mu^* = \mu/\sqrt{4\pi\epsilon_0\epsilon\sigma}$ and $q^* = q/\sqrt{4\pi\epsilon_0\epsilon\sigma}$ to non-dimensionalise dipole moment and charge and set both $4\pi\epsilon_0$ and μ^* to unity. The colloidal bead-solvent interactions were modelled with a LJ potential using the same parameters, ϵ and σ, as for the solvent-solvent interactions, and both solvent particles and colloidal beads have the same mass m. Electrostatic interactions were treated with Ewald summation and tin-foil boundary conditions[16]. Cutoff radii for all LJ and real space Coulomb interactions were set to 8σ and the k-space settings were chosen such that the relative accuracy of the force was approximately 10^{-5}, as estimated with the formulas provided in ref. 17. The equations of motion were integrated using a timestep of $\Delta t = 0.002\tau$, where $\tau = \sigma\sqrt{m/\epsilon}$ is the unit of time.

Equilibration. The initial lattice structure was equilibrated in the *NVT* ensemble for a period of $2 \times 10^3\tau$ using a Nosé–Hoover thermostat[18,19] with a relaxation time of 0.5τ and a target temperature of $T_\infty = 1.15\epsilon/k_{\mathrm{B}}$, where k_{B} is the Boltzmann constant which was set to unity. Subsequently, all particle velocities of the last configuration were rescaled to match the average kinetic energy of the *NVT* run, which was followed by a $2 \times 10^3\tau$ long *NVE* equilibration run. A heat flux was then imposed onto the sytsem using the eHEX/a algorithm[13], where the rate of energy supplied to the hot (and withdrawn from the cold) colloid was set to $\mathcal{F} = 52.75\epsilon/\tau$. After waiting for a period of $10^4\tau$ for any transient behaviour to disappear and the system to reach a steady state, we started the $1.5 \times 10^5\tau$ long production run and stored snapshots of the trajectory for further post-processing of translational, kinetic temperature and dipole orientations. In addition, we carried out a $1.5 \times 10^5\tau$ long *NVE* simulation in order to subtract non-vanishing equilibrium averages of the spatially averaged field and the dipolar orientations from the NEMD results. The relative increase in the total energy throughout the entire NEMD production run (75 million timesteps) was approximately 0.14%, which is comparable to the value of 0.12% for the equilibrium production run.

Statistical accuracy. The size of each error bar in Fig. 2c represents twice the standard deviation of the mean value which was calculated as the difference between the non-equilibrium and the equilibrium averages. For the individual production run we computed field averages according to the following protocol: at regular time intervals of $\delta t = 50\Delta t$ we computed $\langle E_{z,\mathrm{TP}}(z) \rangle$ according to equation (6), excluding dipoles within a distance of R_{TP} from the colloid centres. We then averaged $\langle E_{z,\mathrm{TP}}(z) \rangle$ over slabs of width $\Delta z = L/24$ which are centred around the points $z_i = -L/2 + (i - 1/2)\Delta z$, where $i = 1, \ldots, 24$. The resulting instantaneous spatial averages are denoted by E_i^m, where $m = 1, \ldots, M$ indexes the simulation time according to $t^m = m\delta t$ and $M = 1.5 \times 10^6$ is the total number of configurations considered. From the resulting time series $\{E_i^1, \ldots, E_i^M\}$ we computed the mean value, $\bar{E}_i$, for each bin and estimated its standard deviation, $\bar{\sigma}_i$, using block average analysis. Errors for the final results $\bar{E}_{i,\mathrm{TP}} = \bar{E}_{i,\mathrm{NEMD}} - \bar{E}_{i,\mathit{NVE}}$ shown in the plot were calculated as the square root of the total variance $\bar{\sigma}_{i,\mathrm{NEMD}}^2 + \bar{\sigma}_{i,\mathit{NVE}}^2$, assuming that the production runs were statistically independent. The quantity $\tilde{E}$, appearing in equation (5), was computed from the slabs with index $j \in \{1, 2, 11, 12, 13, 14, 23, 24\}$ using the relation $\tilde{E} = -1/8 \sum_j |\bar{E}_{j,\mathrm{TP}}|$. These slabs correspond to the region of constant average field between the colloids. Errors were propagated assuming that the terms in the sum are statistically independent such that the error $\sigma_{\tilde{E}}$ is given by the square root of $1/8 \sum_j \bar{\sigma}_{j,\mathrm{TP}}^2$. The estimate of q_{TP} follows from multiplication of $\tilde{E}$ by the constant factor $2A\epsilon_0$. The error bar for the estimate of q_{TP} obtained with equation (4) is omitted since we do not have error estimates for the temperature contour lines shown in Fig. 1a. The computation of S_{TP} involves additional simulation data and is explained in Appendix C.

Appendix A: Analytical model for the field

In this section we derive the analytical model proposed in equation (5). To this end, we first show how the spatial average of the three-dimensional field, $\langle E_z(z) \rangle$, calculated from the full charge density, $\rho(\boldsymbol{r})$, is related to the one-dimensional field, $E_{\mathrm{1D}}(z)$, calculated from the spatially averaged charge density, $\rho_{\mathrm{1D}}(z)$. The subscript $_{\mathrm{TP}}$ used in the main text is dropped for notational convenience. We consider periodic boundary conditions (PBCs) and understand that this is implicitly taken into account whenever an expression of the form $\boldsymbol{r} - \tilde{\boldsymbol{r}}$ is evaluated.

For an arbitrary charge distribution, the field can be calculated as

$$\boldsymbol{E}(\boldsymbol{r}) = -\kappa \nabla_{\boldsymbol{r}} \int_\Omega \mathrm{d}^3\tilde{r}\, G(\boldsymbol{r} - \tilde{\boldsymbol{r}})\rho(\tilde{\boldsymbol{r}}), \tag{A1}$$

where $\kappa = (4\pi\epsilon_0)^{-1}$ with ϵ_0 being the vacuum permittivity, $\nabla_{\boldsymbol{r}} = (\partial_x, \partial_y, \partial_z)$ is the gradient in Cartesian coordinates, Ω denotes the orthogonal simulation box of volume $V = L_x L_y L_z$ and $G(\boldsymbol{r} - \tilde{\boldsymbol{r}})$ is a modified kernel that takes into account periodicity[6]. Averaging the z-component of the field over planes perpendicular to the z-axis yields[6,20]

$$\langle E_z(z) \rangle = \frac{1}{L_x L_y} \int_{-\frac{L_x}{2}}^{\frac{L_x}{2}} \int_{-\frac{L_y}{2}}^{\frac{L_y}{2}} \mathrm{d}x\mathrm{d}y\, E_z(\boldsymbol{r}) \tag{A2a}$$

$$= -\kappa \frac{\partial}{\partial z} \int_{-\frac{L_z}{2}}^{\frac{L_z}{2}} \mathrm{d}\tilde{z}\, \underbrace{\frac{1}{L_x L_y} \int_{-\frac{L_x}{2}}^{\frac{L_x}{2}} \int_{-\frac{L_y}{2}}^{\frac{L_y}{2}} \mathrm{d}\tilde{x}\mathrm{d}\tilde{y}\, \rho(\tilde{\boldsymbol{r}})}_{= \rho_{\mathrm{1D}}(\tilde{z})}$$

$$\times \underbrace{\int_{-\frac{L_x}{2}}^{\frac{L_x}{2}} \int_{-\frac{L_y}{2}}^{\frac{L_y}{2}} \mathrm{d}x\mathrm{d}y\, G(\boldsymbol{r} - \tilde{\boldsymbol{r}})}_{= G_{\mathrm{1D}}(z-\tilde{z})} \tag{A2b}$$

$$= -\kappa \int_{-\frac{L_z}{2}}^{\frac{L_z}{2}} \mathrm{d}\tilde{z}\, G_{\mathrm{1D}}'(z - \tilde{z})\rho_{\mathrm{1D}}(\tilde{z}) \tag{A2c}$$

$$= \frac{1}{\epsilon_0} \int_{-\frac{L_z}{2}}^{z} \mathrm{d}\tilde{z}\, \rho_{\mathrm{1D}}(\tilde{z}) + \frac{1}{\epsilon_0} \underbrace{\frac{1}{L_z} \int_{-\frac{L_z}{2}}^{\frac{L_z}{2}} \mathrm{d}\tilde{z}\, \tilde{z}\rho_{\mathrm{1D}}(\tilde{z})}_{= P_z} \tag{A2d}$$

$$= E_{\mathrm{1D}}(z), \tag{A2e}$$

where

$$G_{\mathrm{1D}}(z) = 2\pi \left[-|z| + \frac{z^2}{L_z} + \frac{L_z}{6} \right] \tag{A3}$$

is the spatially averaged kernel for PBCs and P_z the z-component of the average box dipole density.

Next, we work out the averaged charge density and compute the field from equation (A2d). The colloids are modelled by two homogeneously charged, spherical shells of radius R (in the main text we refer to this quantity as R_{TP}). Since all equations involved are linear, we can decompose the problem and focus on a single colloid. If we centre the charge distribution of this colloid around the origin, we can formulate the charge density as

$$\rho^{(1)}(\boldsymbol{r}) = \frac{q}{4\pi R^2}\delta(r - R), \tag{A4}$$

where $q = \int_\Omega \mathrm{d}^3 r \rho^{(1)}(\boldsymbol{r})$ is the total charge, r the distance from the origin and $\delta(r - R)$ the Dirac delta function. Let us assume that $2R < L_x = L_y \leq L_z$ such that the charge distribution is fully contained within the reference box. We then have the freedom to integrate over the largest inscribed cylinder and obtain

$$\rho_{1D}^{(1)}(z) = \frac{1}{L_x L_y} \int\limits_{-\frac{L_x}{2}}^{\frac{L_x}{2}} \int\limits_{-\frac{L_y}{2}}^{\frac{L_y}{2}} \mathrm{d}x\mathrm{d}y \, \rho(\boldsymbol{r}) \tag{A5a}$$

$$= \frac{q}{2R^2 L_x L_y} \int\limits_{0}^{L_x/2} s\mathrm{d}s \, \delta\left(\sqrt{s^2 + z^2} - R\right), \tag{A5b}$$

where $r = \sqrt{s^2 + z^2}$. Employing a second transformation, $\tau = \sqrt{s^2 + z^2}$ with $s\mathrm{d}s = \tau\mathrm{d}\tau$, it is straightforward to solve the above integral to find

$$\rho_{1D}^{(1)}(z) = \begin{cases} \frac{q}{2RA} & \text{if } |z| < R, \\ 0 & \text{otherwise,} \end{cases} \tag{A6}$$

where $A = L_x L_y$ is the cross-sectional area. The averaged charge density taking into account both colloids centred around z_h and z_c, respectively, is therefore given by the piecewise constant function

$$\rho_{1D}(z) = \frac{q}{2RA} \begin{cases} +1 & \text{if } |z - z_h| < R, \\ -1 & \text{if } |z - z_c| < R, \\ 0 & \text{otherwise.} \end{cases} \tag{A7}$$

If we plug this result into equation (A2d) and carry out the integration, we obtain the final result

$$\frac{\langle E_z(z)\rangle}{\tilde{E}} = \begin{cases} -1 & \text{if } |z| > z_c + R, \\ +1 & \text{if } |z| < z_c - R, \\ (z - z_h)/R & \text{if } |z - z_h| \leq R, \\ (z_c - z)/R & \text{otherwise,} \end{cases} \tag{A8}$$

where $\tilde{E} = q/(2\epsilon_0 A)$ is the constant field value for the region between the two colloids.

The quantity $\tilde{E}$ can be understood easily by applying Gauss's theorem to the blue control volume shown in Fig. A1. The charge q in the centre represents the thermally induced charge of the hot colloid. Let us denote the surface of this volume by $\partial\Gamma$, the union of the two faces highlighted in blue by $\partial\Gamma_\parallel$, and the union of the remaining faces by $\partial\Gamma_\perp$. According to Gauss's theorem the total charge enclosed by $\partial\Gamma$ is related to the field flux through $\partial\Gamma$ such that

$$\oiint\limits_{\partial\Gamma} \boldsymbol{E}(\boldsymbol{r}) \cdot \mathrm{d}\boldsymbol{S} = \frac{q}{\epsilon_0}, \tag{A9}$$

where $\mathrm{d}\boldsymbol{S}$ is the surface normal vector. If we decompose the surface integral and recall that the surface normal vector is perpendicular to the field on $\partial\Gamma_\perp$ due to the periodic setup, we find

$$\oiint\limits_{\partial\Gamma} \boldsymbol{E}(\boldsymbol{r})\cdot\mathrm{d}\boldsymbol{S} = \iint\limits_{\partial\Gamma_\parallel} \boldsymbol{E}(\boldsymbol{r})\cdot\mathrm{d}\boldsymbol{S} + \underbrace{\iint\limits_{\partial\Gamma_\perp} \boldsymbol{E}(\boldsymbol{r}) \cdot \mathrm{d}\boldsymbol{S}}_{=0} = \langle E_{z,\parallel}\rangle 2A = \frac{q}{\epsilon_0}. \tag{A10}$$

Rearranging terms, we find

$$\tilde{E} = \langle E_{z,\parallel}\rangle = \frac{q}{2\epsilon_0 A}, \tag{A11}$$
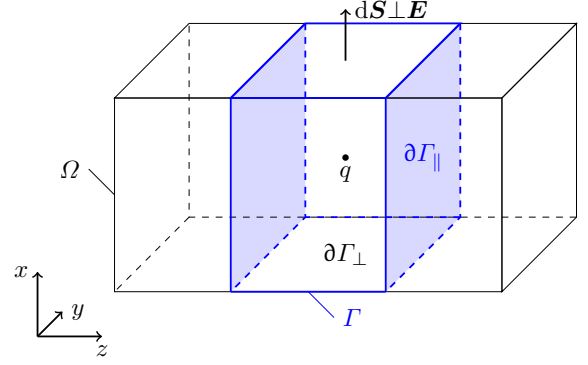
which is our final result.

FIG. A1. Illustration of the simulation box Ω containing a charge q located at the centre of a control volume Γ (solid and dashed blue lines) to which we apply Gauss's theorem. For the two faces of Γ denoted by $\partial\Gamma_\parallel$ (highlighted in blue) the field $\boldsymbol{E}$ has a contribution parallel to the surface normal vector $\mathrm{d}\boldsymbol{S}$, whereas it is orthogonal to it on all other faces denoted by $\partial\Gamma_\perp$.
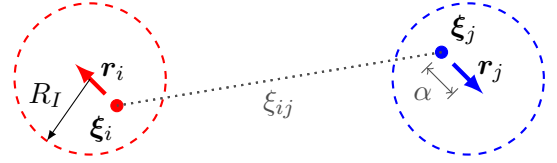

FIG. B1. Two solvent particles with dipoles (coloured arrows) located at $\boldsymbol{r}_i$ and $\boldsymbol{r}_j$, respectively, and displaced LJ centres, $\boldsymbol{\xi}_i$ and $\boldsymbol{\xi}_j$, separated by a distance of ξ_{ij}. The mass of a solvent particle is distributed homogeneously over a ball of radius R_I, as illustrated by the dashed circles. The asymmetry in the short-ranged interactions, as compared to the Stockmayer model, is controlled by the parameter α.

We note that the value of $\tilde{E}$ is constant and does not change if we move the surfaces $\partial\Gamma_\parallel$ along the z-axis as long as they enclose the charge entirely. Finally, we note that the presence of the opposite charge $-q$ is already taken into account implicity, which is indicated by the multiplication by twice the cross-sectional area A in equation (A10). Equivalently, we can think of the result as the sum of two equal contributions, half from the charge q and the other half from $-q$.

Appendix B: Off-centre Stockmayer Model

Displacing the Lennard-Jones (LJ) centre from the location of the point dipole leads to modified forces and torques as compared to the original Stockmayer model[7]. We note that electrostatic contributions are not affected by this modification and refer to ref. 21 for the relevant expressions. All modifications of short-ranged interactions related to the perturbation of the LJ centre are governed by a single parameter α and summarised in this section.

Let us consider the short-ranged, pairwise interactions between two solvent particles as illustrated in Fig. B1. The point dipoles of mass m are located at the positions $\boldsymbol{r}_i$ and $\boldsymbol{r}_j$, respectively. The mass is distributed homogenously over a ball of radius $R_I = \sigma/2$ such that the moment of inertia is given by $I = 2mR_I^2/5$, which corresponds to $I^* = 0.1$ in reduced units. The LJ centre is denoted by $\boldsymbol{\xi}$ and displaced from the position of the dipole by a vector $\Delta\boldsymbol{r} = \boldsymbol{\xi} - \boldsymbol{r} = \alpha\hat{\boldsymbol{\mu}}$, where $\hat{\boldsymbol{\mu}}$ is the unit vector of the dipole moment $\boldsymbol{\mu}$. The quantity α allows us to control the level of asymmetry, i.e. the perturbation to the original Stockmayer model, and we employed a

value of $\alpha = -\sigma/4$ in all our simulations.

The radially symmetric, pairwise LJ potential is given by

$$u(r) = 4\epsilon \left[\left(\frac{\sigma}{r} \right)^{12} - \left(\frac{\sigma}{r} \right)^{6} \right], \tag{B1}$$

where ϵ is the unit of energy. For performance reasons, we employed a cutoff of $r_{\mathrm{c}} = 8\sigma$ for all short-ranged interactions. The energy contribution for the two particles shown in Fig. B1 is therefore given by $u_{ij} = u(\xi_{ij})\Theta(r_{\mathrm{c}} - \xi_{ij})$, where $\Theta(r)$ is the Heaviside function and $\boldsymbol{\xi}_{ij} = \boldsymbol{\xi}_j - \boldsymbol{\xi}_i$. Taking the negative gradient of the energy with respect to $\boldsymbol{\xi}_i$ and applying a cutoff, we obtain the force

$$\boldsymbol{f}_{ij} = \Theta(r_{\mathrm{c}} - \xi_{ij}) 24\sigma\epsilon \left[\left(\frac{\sigma}{\xi_{ij}} \right)^{6} - 2 \left(\frac{\sigma}{\xi_{ij}} \right)^{12} \right] \frac{\boldsymbol{\xi}_{ij}}{\xi_{ij}^2} \tag{B2}$$

acting on particle i with the corresponding force $\boldsymbol{f}_{ji} = -\boldsymbol{f}_{ij}$ acting on particle j. The short-ranged contributions to the torques acting on these particles are then simply given by

$$\boldsymbol{\tau}_{ij} = \alpha \hat{\boldsymbol{\mu}}_i \times \boldsymbol{f}_{ij} \tag{B3}$$

and

$$\boldsymbol{\tau}_{ji} = \alpha \hat{\boldsymbol{\mu}}_j \times \boldsymbol{f}_{ji}, \tag{B4}$$

respectively, where $\times$ denotes the cross product between two vectors. In the limit $\alpha \to 0$ these torque contributions vanish such that we recover the original Stockmayer model.

Appendix C: Estimation of S_{TP}

We estimated the thermo-polarisation coefficient using the relation

$$S_{\mathrm{TP}}(z) = \frac{\langle E_{z,\mathrm{TP}}(z) \rangle}{\partial_z \langle T(z) \rangle}, \tag{C1}$$

where $\partial_z \langle T(z) \rangle$ denotes the gradient of the temperature averaged over planes perpendicular to the z-axis (see Fig. C1). The simulation data reveals a perfectly linear profile in the vicinity of the origin, such that $\beta \equiv \partial_z \langle T(z) \rangle$ is constant. We recall that the field value is $\tilde{E}$ in that region (see Fig. 1), implying that S_{TP} is effectively a constant. Propagating the errors of $\tilde{E}^* = (-1.96 \pm 0.20) \times 10^{-3}$ and $\beta^* = (-9.09 \pm 0.03) \times 10^{-3}$ according to

$$\sigma_S = \frac{1}{|\beta|} \sqrt{\sigma_{\tilde{E}}^2 + S_{\mathrm{TP}}^2 \sigma_\beta^2}, \tag{C2}$$

we obtain an estimate of $S_{\mathrm{TP}}^* = (0.216 \pm 0.022)$ for our model in the temperature and density regions shown in Fig. C1.
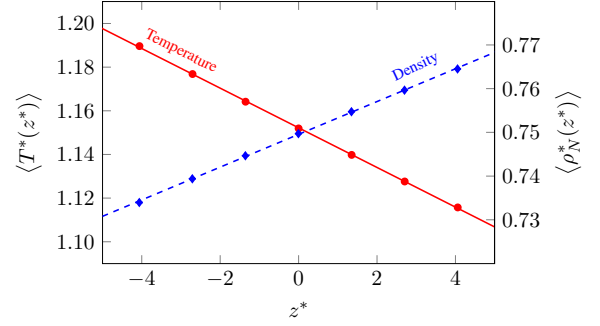

FIG. C1. Temperature (red circles) and solvent number density (blue diamonds) averaged over slabs perpendicular to the z-axis in the vicinity of the origin. The width of each slab is $\Delta z^* = L^*/31$ and all error bars are smaller than the symbol sizes. To estimate errors of the linear fit coefficients for the interval shown in the plot, we first divided the NEMD trajectory into 1500 blocks and performed individual fits for each block average. We then calculated the mean values and standard deviations of the resulting coefficients using block average analysis. The results are $\langle T^*(z^*) \rangle = (-9.09 \pm 0.03) \times 10^{-3} z^* + (1.1522 \pm 0.0002)$ (solid red line) and $\langle \rho_N^*(z^*) \rangle = (3.76 \pm 0.02) \times 10^{-3} z^* + (0.74952 \pm 0.00005)$ (dashed blue line).

REFERENCES

[1] D. Frenkel, J. Phys. Chem. B **120**, 5987 (2016).
[2] F. Bresme, A. Lervik, D. Bedeaux, and S. Kjelstrup, Phys. Rev. Lett. **101**, 020602 (2008).
[3] F. Römer, F. Bresme, J. Muscatello, D. Bedeaux, and J. M. Rubí, Phys. Rev. Lett. **108**, 105901 (2012).
[4] J. Armstrong and F. Bresme, Phys. Rev. E **92**, 060103 (2015).
[5] A. A. Lee, Soft Matter (2016), 10.1039/C6SM01927G.
[6] P. Wirnsberger, D. Fijan, A. Šarić, M. Neumann, C. Dellago, and D. Frenkel, J. Chem. Phys. **144**, 224102 (2016).
[7] W. H. Stockmayer, J. Chem. Phys. **9**, 398 (1941).
[8] J. Muscatello, F. Römer, J. Sala, and F. Bresme, Phys. Chem. Chem. Phys. **13**, 19970 (2011).
[9] J. A. Armstrong and F. Bresme, J. Chem. Phys. **139**, 014504 (2013).
[10] C. D. Daub, P.-O. Åstrand, and F. Bresme, Phys. Chem. Chem. Phys. **16**, 22097 (2014).
[11] C. D. Daub, P.-O. Åstrand, and F. Bresme, Mol. Phys. (2016), 10.1080/00268976.2016.1229058.
[12] I. Iriarte-Carretero, M. A. Gonzalez, J. Armstrong, F. Fernandez-Alonso, and F. Bresme, Phys. Chem. Chem. Phys. **18**, 19894 (2016).
[13] P. Wirnsberger, D. Frenkel, and C. Dellago, J. Chem. Phys. **143**, 124104 (2015).
[14] H. J. C. Berendsen, J. R. Grigera, and T. P. Straatsma, J. Phys. Chem. **91**, 6269 (1987).
[15] S. Plimpton, J. Comput. Phys. **117**, 1 (1995).
[16] S. W. de Leeuw, J. W. Perram, and E. R. Smith, Proc. R. Soc. A **373**, 27 (1980).
[17] Z. Wang and C. Holm, J. Chem. Phys. **115**, 6351 (2001).
[18] S. Nosé, J. Chem. Phys. **81**, 511 (1984).
[19] W. G. Hoover, Phys. Rev. A **31**, 1695 (1985).
[20] I.-C. Yeh and A. Wallqvist, J. Chem. Phys. **134**, 055109 (2011).
[21] A. Toukmaji, C. Sagui, J. Board, and T. Darden, J. Chem. Phys. **113**, 10913 (2000).